

Micromagnetics of the single-domain state of square ferromagnetic nanostructures

R. P. Cowburn* and M. E. Welland

*Nanoscale Science Group, Department of Engineering, University of Cambridge, Trumpington Street,
Cambridge CB2 1PZ, United Kingdom*

(Received 14 April 1998; revised manuscript received 10 June 1998)

Using numerical micromagnetics we have studied the potential energy surface in the vicinity of the two principal remanent near single-domain states of nanoscale square-planar magnetic elements (magnetic nanostructures). We find that there is no metastability and therefore at any finite temperature the nanostructure must adopt its ground state. We have derived an analytical solution to the micromagnetic equations describing the properties of the near single-domain states by treating them as a small perturbation from the uniformly magnetized case. The analytical solution shows that the energy surface between the states can be described by a fourfold symmetric configurational anisotropy field, which can be several hundred Oersteds in strength and which changes sign at a critical width to thickness aspect ratio. The analytical model gives good physical insight into the origin of the configurational anisotropy and predicts a discontinuous transition with diverging susceptibility to occur at the critical aspect ratio. [S0163-1829(98)02838-0]

INTRODUCTION

The magnetism of reduced dimensionality structures has in recent years generated much experimental and theoretical interest. Reduced dimensionality in this context means that one or more of the sample dimensions is small or comparable to the exchange length of the material, which is of the order of ten nanometers for common ferromagnetic materials.

Two-dimensional (2D) magnetism has been extensively studied in thin and ultrathin films and multilayers, leading to the discovery of several magnetic phenomena such as strong surface anisotropies, enhanced moments, and oscillatory interlayer exchange coupling.¹ Advanced lithographic techniques such as electron beam or x-ray lithography or other nanoscale assembly techniques are now opening up the possibility of studying 1D and 0D magnets in the form of magnetic wires and dots.²

Theoretical modeling is an essential part of studying such structures. The semiclassical formalism of micromagnetics is an excellent tool for doing so.^{3,4} Except in special cases where the demagnetizing field is uniform, analytical solution of the micromagnetic equations is rare. Recent advances in computing power, however, have now made numerical solution feasible. Cuboidal particles⁵ and 2D plates⁶ have both been studied by various workers using numerical micromagnetics as well as more applied problems in data storage technology.⁷

Brown's fundamental theorem⁸ states that as the length-scale of a magnetic particle is reduced, there comes a point at which the competition between exchange energy and magnetostatic energy requires that a uniform magnetization distribution be adopted. The fundamental theorem was found not to be rigorously true for nonellipsoidal particles such as cubes and prisms,⁹ but can be made so if "uniform magnetization" is replaced by "near-uniform magnetization." In a recent paper,¹⁰ we showed theoretically that square-planar elements show unexpectedly complex behavior in this near single-domain regime, undergoing transitions through up to

three different near single-domain states as the element size and thickness is varied. In addition to the fundamental interest in studying phase transitions in these reduced dimensionality nanostructures, a precise understanding of the near single-domain states is essential for potential technological applications, such as patterned media for high density data storage¹¹ or magnetoelectronic devices¹² (e.g., magnetic memory chips, spin transistors, and hard-disk read heads). Studying the deviations from uniform magnetization of small cuboidal elements is also important in further understanding the long standing Brown's paradox,¹³ which notes the discrepancy between the nucleation fields predicted by rigorous analytical micromagnetic nucleation theory and many experimentally measured coercive fields.

In this paper we present the results of a detailed study of the two principal near single-domain states of square-planar magnetic elements (nanostructures). In the first section we use numerical micromagnetics to investigate the nature of the potential energy surface around the single-domain states. In the second section we present an analytical solution to the micromagnetic equations for small cuboids within the framework of perturbation theory. These studies together predict the existence of a strong anisotropy within the nanostructures, which we name a configurational anisotropy. This anisotropy field can be several hundred Oe's in strength, changes sign at a critical width to thickness aspect ratio, and will dominate the magnetic behavior of the nanostructures.

NUMERICAL SIMULATIONS

A. Numerical method

We have considered a series of square elements which can be modeled using finite element methods as an ensemble of cubic cells placed on a simple cubic lattice. The meshing density was always chosen such that the elements were at least 2 cells thick, and the size of each cell was less than half the exchange length. We checked that the final energy calculated by the simulation converged with increasing meshing

density, and used the form of the convergence to estimate the size of the error caused by finite meshing density. This was generally less than 5%.

The exchange energy of a given magnetization distribution is given by

$$U_{ex} = \frac{A}{M_s^2} \int |\nabla M_x(\underline{r})|^2 + |\nabla M_y(\underline{r})|^2 + |\nabla M_z(\underline{r})|^2 d^3r, \quad (1)$$

where A is the exchange stiffness, M_s is the saturation magnetization, and $M_i(\underline{r})$ is the Cartesian component of magnetization at position \underline{r} in the element. We have implemented this in discrete mathematics by

$$U_{ex} = \frac{1}{2} A V^{1/3} \sum_i \sum_j \sin^2 \theta_i (\phi_j - \phi_i)^2 + (\theta_j - \theta_i)^2, \quad (2)$$

where V is the volume of each cell and $\{\phi_i, \theta_i\}$ are the spherical polar coordinates of the magnetization direction in the i th cell. The magnitude of the magnetization within a cell is always the saturation magnetization M_s .

The magnetostatic energy of a magnetization distribution is calculated by evaluating the demagnetizing field $H^d(\underline{r})$ at every point in the element, and then calculating the resulting energy in the continuum limit according to

$$U_d = -\frac{1}{2} \int \underline{M}(\underline{r}) \cdot \underline{H}^d(\underline{r}) d^3r, \quad (3)$$

which is implemented discretely by

$$U_d = -\frac{1}{2} V \sum_i \underline{M}_i \cdot \underline{H}_i^d. \quad (4)$$

The demagnetizing field itself is calculated from a convolution of the magnetization with the three-dimensional LaBonte interaction matrix.¹⁴

Boundary cells are treated slightly differently in calculating the exchange energy. The cell on the opposite side of a free face is counted twice in performing the summation of Eq. (3). This is equivalent to assuming a uniform magnetization gradient all the way through the boundary cell.

Once able to calculate the energy of a given magnetization distribution, we then use the method of steepest descent to find the set of $\{\{\phi_i, \theta_i\}\}$ which minimizes the total energy. As is characteristic of any hysteretic system, the starting conditions of the minimization can influence which energy minimum is eventually found. We shall make use of this important point later in the paper.

B. Numerical results

We showed previously¹⁰ using numerical micromagnetics that there are two principal near single-domain magnetization distributions relevant to small square-planar elements. We have named these ‘‘flower’’ and ‘‘leaf’’ and present them in Fig. 1 for reference. Elements small enough to adopt a near single-domain state (as opposed to a vortex or buckled state) as the ground state display either the flower or the leaf configuration, depending on the width to thickness aspect ratio of the element. Elements with aspect ratio less than 2.7 were found to have a flower ground state whereas those with

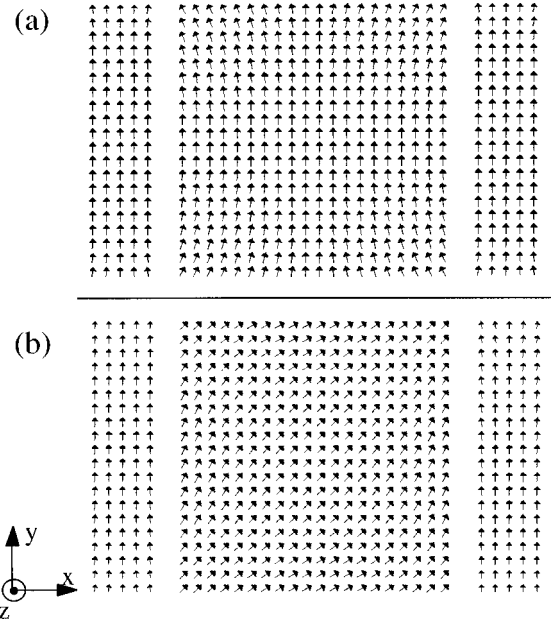


FIG. 1. Examples of the magnetization vectors in (a) the flower and (b) the leaf magnetization distribution in $60 \times 60 \times 15$ nm nanostructures. The central part shows a plan view, whereas the side parts show the left and right side surfaces.

aspect ratio greater than 2.7 had a leaf ground state. The fact that a particular state might be the ground state is no guarantee, however, that it will be observed as the remanent state of the nanostructure. Metastability is a common feature of magnetic systems. In order to know if the predicted ground state is an accurate prediction of the state which will be observed in a nanostructure in zero field, it is necessary to study the potential energy surface in the vicinity of the two near single-domain states. Knowledge of the shape of the energy surface is also important if one is to understand the static and temporal spin-reversal behavior of the nanostructure.

We have started our investigation with a square-planar element of size $20 \times 20 \times 10$ nm, for which the ground state is the flower. In order to provide a ready link with the large amount of experimental work which is emerging in this field, we have assigned values to M_s and A which are characteristic of the magnetic alloy Permalloy ($\text{Ni}_{80}\text{Fe}_{20}$, for which $M_s = 800$ emu cm^{-3} and $A = 1.05 \times 10^{-6}$ erg cm^{-1}). Our results can be applied to other soft isotropic magnetic materials by scaling all lengths by $\sqrt{A/M_s}$ and all energy densities per moment by M_s . We have then used our code to minimize the energy of the element with different starting conditions. We always start with a uniform distribution (i.e., all moments parallel), but vary the in-plane direction. We find that irrespective of the starting direction (within one octant), the element always minimizes towards a mean in-plane magnetization direction of 90° , which corresponds to the flower distribution. Even starting with the magnetization aligned to within 0.1° of the mean direction of the leaf distribution (i.e., $\phi = 45.1^\circ$) lead to a coherent rotation of the magnetization to the flower distribution. This is highly indicative of the leaf state being an energy maximum and not a metastable minimum for this size element.

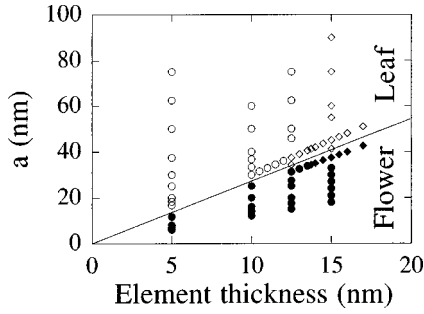


FIG. 2. A phase diagram of numerical simulation results, showing as a function of element size and thickness the finally attained equilibrium state. The solid line has gradient 2.7 and shows the boundary between the flower and leaf ground states. For each simulation, a uniformly magnetized state 0.1° away from the nonground state direction was used as the starting condition. ● indicates flower, ○ indicates leaf, ◆ indicates pseudoflower, ◇ indicates pseudoleaf.

We then studied a slightly larger element of size $33.3 \times 33.3 \times 10$ nm. Such an element, having an aspect ratio of 3.33, is located on the other side of the flower-leaf phase boundary and so has the leaf distribution as its ground state. This time the element always moved towards $\langle \phi \rangle = 45^\circ$ and hence the leaf distribution, even when started within 0.1° of the mean flower direction. The flower state must therefore be an energy maximum and not a metastable minimum.

The two elements which we have so far studied have thus been free of metastability. We checked that this result was independent of the meshing density. In order to see if this is a general feature of all small, square-planar elements, we have performed a slightly reduced version of this experiment on a number of different sized elements. For each element we have determined its ground-state distribution (i.e., flower or leaf) from its aspect ratio. We have then started a minimization from a uniformly magnetized state 0.1° away from the mean direction of the *other* state and monitored the minimization. The final equilibrium state (i.e., flower or leaf) was then recorded. Figure 2 summarizes the results by showing as a function of element size and thickness the final equilibrium state. The flower-leaf ground-state phase boundary line has also been superimposed. For elements of thickness less than 12 nm, one sees that the final equilibrium state (as represented by the points) always follows the ground state, even though the starting conditions of the minimization were chosen to encourage selection of the other state. For elements thicker than 12 nm, the phase diagram shows the presence of pseudoflower and pseudoleaf states. These states are the basic flower and leaf states with lower reflection symmetry. Figure 3 shows an example of a pseudoflower and a pseudoleaf state. In the case of the pseudoflower shown, the mean in-plane magnetization direction is $\langle \phi \rangle = 76^\circ$, compared with the full flower value of 90° . In the case of the pseudoleaf shown, $\langle \phi \rangle = 63^\circ$, compared with the full leaf value of 45° . The pseudoflower can be described as a full flower with a small amount of leaf character and the pseudoleaf can be described as a full leaf with a small amount of flower character. This makes the transition between the flower and leaf states *continuous* when pseudostates are involved, which is to be contrasted with the abrupt transition which occurs at smaller thicknesses (i.e.,

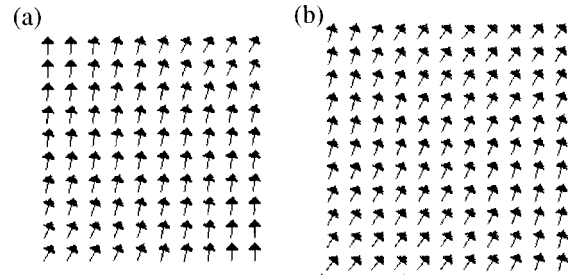


FIG. 3. Examples of the magnetization vectors in (a) the pseudoflower and (b) the pseudoleaf states, in a $37.5 \times 37.5 \times 15$ nm and $41.25 \times 41.25 \times 15$ nm element, respectively.

< 12 nm) which do not involve pseudostates. We checked when the minimization terminated on a pseudostate that the pseudostate was of lower energy than the corresponding full state. This was always the case. Thus even though the ground state may not be as simple as a full flower or leaf, it is a general principle of these small square-planar elements that metastability is always absent. The ground-state phase diagram (when correctly calculated to also involve pseudostates) should thus always be a good prediction of the remanent state of the element.

It has long been known that a square, *single-domain* (i.e., truly single domain, with perfectly uniform magnetization) element cannot exhibit any in-plane shape anisotropy. The fact that we observe energy differences between the leaf ($\langle \phi \rangle = 45^\circ$) and the flower ($\langle \phi \rangle = 90^\circ$) means that there is some dependence of energy on the in-plane net magnetization direction which must therefore come about as a result of the nonuniformity of the magnetization distribution within the near single-domain state. A close examination of Fig. 1 shows that there is some bending of the magnetization in the vicinity of the element edges. If we are to explain the ground-state diagram it is therefore necessary to understand the influence of nonuniformity on the effective shape anisotropy.

C. Analytical modeling

Analytical solution of micromagnetic problems is comparatively rare because generally it involves finding the solution to nonlinear differential equations. Analytical solutions to Brown's fundamental theorem critical size¹⁵ and the nucleation problem¹⁶ have been presented for the special cases of ellipsoidal particles which generate uniform demagnetizing fields. The nonuniform demagnetizing field within nonellipsoidal bodies has also been calculated.¹⁷ Recently, the many soliton solution of the imaginary time sine Gordon equation has been used to describe domain structure in rectangular magnetic plates.¹⁸ Analytical solutions are desirable because they often give more physical insight into a problem than a numerical simulation, and they also allow trends to be predicted without the need to repeat the numerical simulation many times. We will show in this section that the near single-domain states so far discussed can be described by a good analytical approximation because they can be treated as a small perturbation from the truly single-domain state. In this case, the micromagnetic equations can be linearized and a solution found. We shall work with two orthogonal basis perturbations, one possessing the symmetry of the flower

state and the other the symmetry of the leaf state. We shall then consider a general state which is a linear combination of the two. The total magnetic energy of the state can then be expressed as a function of the coefficients of the linear combination and the mean in-plane magnetization direction and minimized with respect to these parameters. We are thus able to find analytically the nature of the near single-domain state (i.e., flower- or leaflike) and its energy as a function of element size and aspect ratio.

In addition to providing the solution to a specific problem in nanoscale magnetism, we hope that it might be possible to generalize the formalism presented here to solve many other micromagnetic problems in a variety of particle shapes.

1. The flower perturbation

The flower can be described as a perturbation from a single-domain state oriented parallel to one edge of the square element. If the main magnetization direction is taken to be along the y axis, then the symmetry of the flower is expressed by an in-plane magnetization perturbation directed along the x axis and of a magnitude which depends on some function of the product xy where the coordinates are measured from the center of the square. In addition, we assume an out-of-plane magnetization perturbation directed along the z axis and of a magnitude which depends upon some function of the product yz , where z is also measured from the center of the element. We cannot know *a priori* the exact profile of the magnetization perturbation for this depends on the details of the balance between the local demagnetizing field and the exchange field. We therefore consider a general polynomial expansion. The reflection symmetry of the problem means that even terms are forbidden. It was found sufficient to take terms in xy and $(xy)^3$ for the in-plane perturbation and terms only in yz for the out-of-plane perturbation. We thus write the perturbation for the flower as

$$\begin{aligned}\Delta\phi_F(x,y) &= -\frac{4xy\Delta\phi_F}{a^2} - \frac{64x^3y^3\Delta\phi'_F}{a^6} \\ \Delta\theta_F(y,z) &= \frac{4ryz\Delta\theta_F}{a^2},\end{aligned}\quad (5)$$

where a is the width of the element, a/r is its thickness where r is the width to thickness aspect ratio, and the variables $\Delta\phi_F$, $\Delta\phi'_F$, and $\Delta\theta_F$ represent the overall strength of the linear in-plane, the cubic in-plane, and the linear out-of-plane flower perturbation, respectively.

2. The leaf perturbation

In describing the leaf perturbation, the main magnetization is taken to lie along the leading diagonal of the square element and the in-plane perturbation magnetization follows the nonleading diagonal. Just as for the flower the in-plane perturbation at a given point depended on the distance from the x axis times the distance from the y axis (i.e., the product xy), the leaf in-plane perturbation at a given point is taken to depend on the distance from the leading diagonal times the distance from the nonleading diagonal. Simple geometry shows that this product is described by $x^2 - y^2$. The higher-order polynomial term is in this case taken to be $x^4 - y^4$. For

the out-of-plane case, the symmetry of the distribution requires a perturbation which is linear in z (as measured from the center of the element) and which also is proportional to the distance from the nonleading diagonal. This is achieved by the term $(x+y)z$. Thus, the full leaf perturbation can be written

$$\begin{aligned}\Delta\phi_L(x,y) &= \frac{4}{a^2}(x^2 - y^2)\Delta\phi_L + \frac{16}{a^4}(x^4 - y^4)\Delta\phi'_L, \\ \Delta\theta_L(x,y,z) &= \frac{2r}{a^2}(x+y)z\Delta\theta_L.\end{aligned}\quad (6)$$

3. Energy of the general state

We now construct a general perturbation by taking a linear combination of the two basis perturbations

$$\begin{aligned}\Delta\phi(x,y) &= \Delta\phi_F(x,y) + \Delta\phi_L(x,y), \\ \Delta\theta(x,y,z) &= \Delta\theta_F(x,y,z) + \Delta\theta_L(x,y,z).\end{aligned}\quad (7)$$

There is no need to write linear combination coefficients in Eq. (7) because they can be absorbed into $\Delta\phi_F, \Delta\phi'_F, \Delta\theta_F$ and $\Delta\phi_L, \Delta\theta'_L, \Delta\theta_L$ of Eqs. (5) and (6). In addition to these six free parameters, we must also consider the mean in-plane magnetization direction $\langle\phi\rangle$. The magnetic energy of this general state is given by the sum of its exchange energy and its magnetostatic energy.

The mean exchange energy density of the nanostructure is given by evaluating Eq. (1) for the perturbation $\Delta\phi(x,y), \Delta\theta(x,y,z)$ and then dividing by the element volume, which gives

$$\begin{aligned}\bar{E}_{\text{ex}} &= \frac{4A}{105a^2} \left\{ 2(35\Delta\phi_F^2 + 42\Delta\phi_F\Delta\phi'_F + 27\Delta\phi_F'^2) \right. \\ &\quad + 8(35\Delta\phi_L^2 + 84\Delta\phi_L\Delta\phi'_L + 60\Delta\phi_L'^2) \\ &\quad \left. + 35(1+r^2) \left(\Delta\theta_F^2 + \Delta\theta_F\Delta\theta_L + \frac{\Delta\theta_L^2}{2} \right) \right\}.\end{aligned}\quad (8)$$

Because the exchange energy density depends only on magnetization *gradients*, the seventh free parameter $\langle\phi\rangle$ (the mean in-plane magnetization direction) does not appear in Eq. (8).

We shall now find an expression for the magnetostatic energy in the element. For a given perturbation in spherical polar coordinates $[\Delta\phi(x,y), \Delta\theta(x,y,z)]$, the corresponding Cartesian perturbation is

$$\underline{\Delta M}(x,y,z) = M_s \begin{bmatrix} -\Delta\phi(x,y)\sin\langle\phi\rangle \\ \Delta\phi(x,y)\cos\langle\phi\rangle \\ \Delta\theta(x,y,z) \end{bmatrix}.\quad (9)$$

In the limit of a small perturbation, the magnetostatic energy density at a point in the nanostructure approximates to

$$E_d(x,y,z) = \underline{\Delta M}(x,y,z) \cdot \underline{N}(x,y,z) M_s \begin{bmatrix} \cos\langle\phi\rangle \\ \sin\langle\phi\rangle \\ 0 \end{bmatrix},\quad (10)$$

where $\underline{N}(x,y,z)$ is the spatially variant demagnetizing tensor for the nanostructure. The terms on the right-hand side of the dot product in the above equation give the local demagnetizing field assuming a uniform magnetization. This will be slightly different from the true local field because what is really required is the local demagnetizing field due to the perturbed distribution. However, the errors are of order $\Delta\phi^2$ and so can be ignored for small perturbations. As was done

for the exchange energy, we integrate the magnetostatic energy density throughout the volume of the element and then divide by the element volume in order to give the total magnetostatic energy as an average magnetostatic energy density. When the demagnetizing tensor is expanded into its individual elements and the reflection symmetry of the basis perturbations used to simplify, the mean magnetostatic energy density is found to be

$$\begin{aligned} \bar{E}_d = \frac{M_s^2 r}{a^3} \int_{-a/2}^{a/2} dx \int_{-a/2}^{a/2} dy \int_{-a/2r}^{a/2r} dz \left\{ \cos 2\langle\phi\rangle N_{12}(x,y,z) \Delta\phi_F(x,y) + \sin\langle\phi\rangle N_{23}(x,y,z) \Delta\theta_F(x,y,z) \right. \\ \left. + \sin 2\langle\phi\rangle \frac{N_{22}(x,y,z) - N_{11}(x,y,z)}{2} \Delta\phi_L(x,y) + (\sin\langle\phi\rangle + \cos\langle\phi\rangle) N_{23}(x,y,z) \Delta\theta_L(x,y,z) \right\}. \end{aligned} \quad (11)$$

We can make use of the scale-invariant nature of the demagnetizing field to rewrite this in the form

$$\begin{aligned} \bar{E}_d = -M_s^2 \{ C_F^\phi \Delta\phi_F \cos 2\langle\phi\rangle \\ + C_F^{\phi'} \Delta\phi_F' \cos 2\langle\phi\rangle + C_F^\theta \Delta\theta_F \sin\langle\phi\rangle \\ + C_L^\phi \Delta\phi_L \sin 2\langle\phi\rangle + C_L^{\phi'} \Delta\phi_L' \sin 2\langle\phi\rangle \\ + C_L^\theta \Delta\theta_L (\sin\langle\phi\rangle + \cos\langle\phi\rangle) \}, \end{aligned} \quad (12)$$

where the spatially invariant factors C_F^ϕ , $C_F^{\phi'}$, and C_F^θ depend *only* on the width to thickness aspect ratio of the element $rand$ are given by

$$\begin{aligned} C_F^\phi &= \frac{r}{a^3} \int_{-a/2}^{a/2} dx \int_{-a/2}^{a/2} dy \int_{-a/2r}^{a/2r} dz \left\{ -\frac{4xy}{a^2} N_{12}(x,y,z) \right\}, \\ C_F^{\phi'} &= \frac{r}{a^3} \int_{-a/2}^{a/2} dx \int_{-a/2}^{a/2} dy \int_{-a/2r}^{a/2r} dz \left\{ -\frac{64x^3y^3}{a^6} N_{12}(x,y,z) \right\}, \\ C_F^\theta &= \frac{r}{a^3} \int_{-a/2}^{a/2} dx \int_{-a/2}^{a/2} dy \int_{-a/2r}^{a/2r} dz \left\{ \frac{4ryz}{a^2} N_{23}(x,y,z) \right\}, \\ C_L^\phi &= \frac{r}{a^3} \int_{-a/2}^{a/2} dx \int_{-a/2}^{a/2} dy \int_{-a/2r}^{a/2r} dz \left\{ \frac{2}{a^2} (x^2 - y^2) \right. \\ &\quad \left. \times [N_{22}(x,y,z) - N_{11}(x,y,z)] \right\}, \\ C_L^{\phi'} &= \frac{r}{a^3} \int_{-a/2}^{a/2} dx \int_{-a/2}^{a/2} dy \int_{-a/2r}^{a/2r} dz \left\{ \frac{8}{a^4} (x^4 - y^4) \right. \\ &\quad \left. \times [N_{22}(x,y,z) - N_{11}(x,y,z)] \right\}, \\ C_L^\theta &= \frac{r}{a^3} \int_{-a/2}^{a/2} dx \int_{-a/2}^{a/2} dy \int_{-a/2r}^{a/2r} dz \left\{ \frac{2r}{a^2} (x+y)z N_{23}(x,y,z) \right\}. \end{aligned} \quad (13)$$

Concern might be expressed over whether some of these integrals converge because the off-diagonal demagnetizing

tensor elements tend to infinity at the corners of a cuboid. We verified that the divergence is of the form $-\ln \varepsilon$ where ε is a measure of the distance from the corner. The divergence is slow so that $\varepsilon^3 \ln \varepsilon$ converges rapidly to zero. The integrals are therefore convergent. A more rigorous analysis of the complete micromagnetic processes which occur at corners has recently been presented by other workers.¹⁹

The closed-form results of these integrals are extremely complex, and so we have evaluated them using numerical integration, presenting the results in Fig. 4. The total energy density ansatz of the general perturbation is then given by the sum of the exchange energy density and the magnetostatic energy density. The true energy density of an element is given by the minimum of \bar{E}_{tot} . Since for a given element \bar{E}_{tot} is only a function of the six perturbation strengths $\Delta\phi_F, \Delta\phi_F', \Delta\theta_F, \Delta\phi_L, \Delta\phi_L', \Delta\theta_L$ and the mean in-plane magnetization direction $\langle\phi\rangle$, the minimization can be

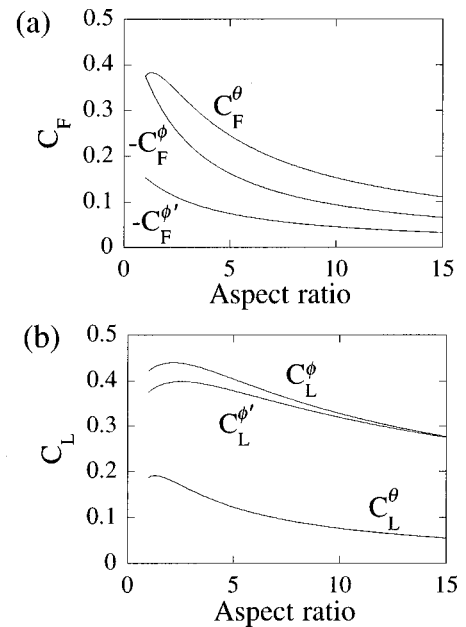


FIG. 4. A numerical evaluation of the C factors as defined in Eq. (13) as a function of width to thickness aspect ratio, r .

achieved by simple analytical methods. The derivative of \bar{E}_{tot} with respect to each of the six perturbation strengths is calculated analytically and set to zero. This yields six equations with three sets of two being coupled. They can thus easily be solved to yield the minimizing values of the perturbation strengths as

$$\begin{aligned}\Delta\phi_F &= \frac{5M_s^2a^2}{128A}(9C_F^\phi - 7C_F^{\phi'})\cos 2\langle\phi\rangle, \\ \Delta\phi'_F &= \frac{-35M_s^2a^2}{384A}(3C_F^\phi - 5C_F^{\phi'})\cos 2\langle\phi\rangle, \\ \Delta\theta_F &= \frac{3M_s^2a^2}{4A(1+r^2)} \\ &\quad \times (C_F^\theta \sin\langle\phi\rangle - C_L^\theta[\sin\langle\phi\rangle + \cos\langle\phi\rangle]), \\ \Delta\phi_L &= \frac{15M_s^2a^2}{512A}(10C_L^\phi - 7C_L^{\phi'})\sin 2\langle\phi\rangle, \\ \Delta\phi'_L &= \frac{-35M_s^2a^2}{1024A}(6C_L^\phi - 5C_L^{\phi'})\sin 2\langle\phi\rangle, \\ \Delta\theta_L &= \frac{3M_s^2a^2}{4A(1+r^2)}[2C_L^\theta(\sin\langle\phi\rangle + \cos\langle\phi\rangle) - C_F^\theta \sin\langle\phi\rangle].\end{aligned}\quad (14)$$

Notice that at this stage we have not yet minimized with respect to $\langle\phi\rangle$; this will be done later. Substituting these minimizing values back into the original energy density ansatz gives the energy density minimum for a given $\langle\phi\rangle$ as

$$\bar{E}_{\text{tot}} = \frac{M_s^4a^2}{A}\{P\cos^2 2\langle\phi\rangle + Q\sin^2 2\langle\phi\rangle + R\}, \quad (15)$$

which can be rewritten as

$$\bar{E}_{\text{tot}} = \frac{M_s^4a^2}{A}\{(Q-P)\sin^2 2\langle\phi\rangle + P+R\}, \quad (16)$$

where the variables P, Q, R depend only on the aspect ratio of the element and are defined as

$$\begin{aligned}P &= \frac{5}{768}(-27C_F^{\phi^2} + 42C_F^\phi C_F^{\phi'} - 35C_F^{\phi'^2}), \\ Q &= \frac{5}{2048}(-60C_L^{\phi^2} + 84C_L^\phi C_L^{\phi'} - 35C_L^{\phi'^2}), \\ R &= \frac{-3}{16(1+r^2)}C_F^{\phi^2}.\end{aligned}\quad (17)$$

P , Q , and R are plotted in Fig. 5 as a function of the element aspect ratio. Notice that in Eq. (16) the part of \bar{E}_{tot} which is proportional to R and therefore expresses the energy contribution of out-of-plane perturbation does not depend upon $\langle\phi\rangle$. This is because the symmetry of the out-of-plane parts of the two basis perturbations is such that they are not orthogonal. Consequently, one can simply show that C_F^θ

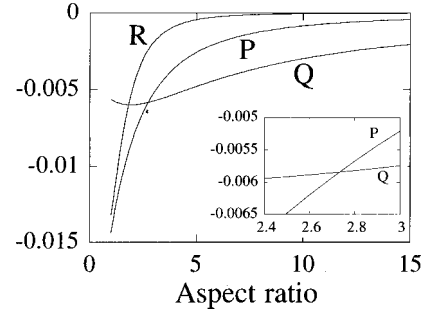


FIG. 5. The functions R , P , and Q as a function of width to thickness aspect ratio, r . Inset is a close up in the vicinity of the intersection of P and Q which corresponds to the transition between flower and leaf states.

$= 2C_L^\theta$, which causes the $\langle\phi\rangle$ dependent parts of R to cancel. We shall return to the physical significance of this later.

The final minimization of Eq. (16) with respect to $\langle\phi\rangle$ is now easily achieved, and yields

$$\begin{aligned}\langle\phi\rangle &= \frac{\pi}{4}, \quad \bar{E}_{\text{tot}} = \frac{M_s^4a^2}{A}(Q+R) \quad \text{for } P > Q, \\ \langle\phi\rangle &= \frac{\pi}{2}, \quad \bar{E}_{\text{tot}} = \frac{M_s^4a^2}{A}(P+R) \quad \text{for } P < Q.\end{aligned}\quad (18)$$

Thus, within the framework of small perturbations, our analytical theory predicts that depending on the element aspect ratio r the ground-state magnetization distribution is either entirely flowerlike ($P < Q$) or is entirely leaflike ($P > Q$). There should not be any mixed (i.e., pseudoflower or pseudoleaf) states. The variation of the energy surface between the two states is of the form $\sin^2 2\langle\phi\rangle$, which describes a fourfold symmetry anisotropy. We name this a configurational anisotropy, for it comes from the different magnetization configurations (i.e., flower or leaf) which occur as the mean in-plane magnetization direction is rotated in the plane. The critical aspect ratio at which $P=Q$ and therefore at which the element ground state changes between the flower and leaf can be read off from the inset of Fig. 5 as 2.733 ± 0.001 which is in excellent agreement with the value of 2.7 ± 0.05 obtained during our numerical simulations.

As well as using the analytic formulas to predict the flower-leaf phase boundary gradient, we can also calculate the magnitude of the configurational anisotropy. We define the in-plane fourfold symmetric configurational anisotropy constant K_1^{config} such that the dependence of energy density on the mean magnetization direction is described by

$$E = \frac{K_1^{\text{config}}}{4}\sin^2 2\langle\phi\rangle. \quad (19)$$

Comparison with Eq. (16) yields immediately the result

$$K_1^{\text{config}} = \frac{4M_s^4a^2}{A}(Q-P), \quad (20)$$

or in terms of an anisotropy field

$$\frac{2K_1^{\text{config}}}{M_s} = \frac{8M_s^3a^2}{A}(Q-P). \quad (21)$$

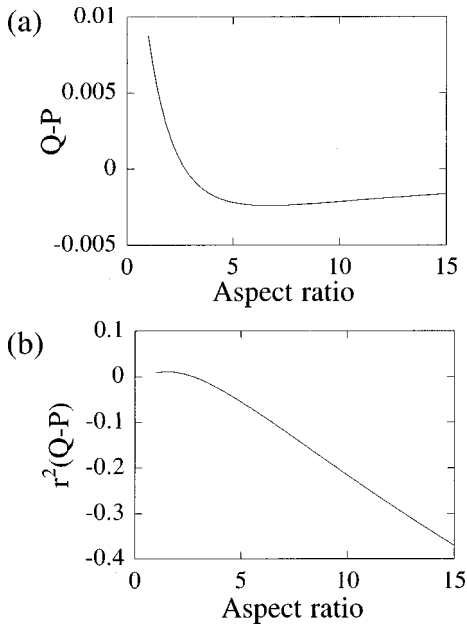


FIG. 6. (a) The function $Q-P$ as a function of width to thickness aspect ratio, r ; (b) the function $r^2(Q-P)$ against r , which has the same form as the dependence of configurational anisotropy on element size at constant thickness.

In Fig. 6 we have plotted $Q-P$ and also $r^2(Q-P)$. The latter, while still being dimensionless, shows the form of the variation of anisotropy field with element size at constant thickness. One sees that the anisotropy field increases almost linearly with element size.

DISCUSSION

A. Comparison of the analytical model with the numerical simulations

It is important to establish that our analytical model reproduces the results obtained by numerical simulations. To this end, we have used the numerical code to find the equilibrium magnetization distribution of a magnetic element with $a=10$ nm and $r=2$. We then found $\Delta\phi(x,y)$ and $\Delta\theta(x,y,z)$ as predicted by the analytical model, and plotted in Fig. 7 a comparison of numerically and analytically determined line sections. One sees that the agreement is very good. This shows that the functions which we chose in Eqs. (5) and (6) to represent the flower and leaf perturbations were suitable.

We then used the numerical code to calculate the total magnetic energy of elements of a variety of sizes and thicknesses. Figure 8 compares the numerical calculation with the analytical values predicted by Eq. (14). The agreement is very good for most of the thickness range shown. At the upper end of the size range the uncertainty in the numerical values increases because of the need to reduce the meshing density in order to limit the total number of cells. One would also expect, however, the analytical model to slightly overestimate the magnitude of the energy at higher sizes for reasons which will be discussed in the following section. Despite these uncertainties, the agreement between the two models is good enough even at larger sizes to be useful.

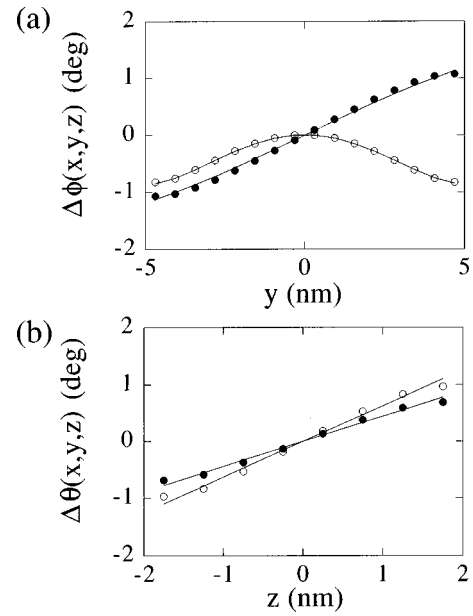


FIG. 7. A comparison between the numerical simulation (solid points indicate flower, open points indicate leaf) and the analytical model (lines) for line sections through a $10 \times 10 \times 5$ nm element. (a) is the in-plane angular perturbation and (b) is the out-of-plane angular perturbation.

There are two other points of agreement between the analytical model and the numerical simulations. The first is the analytical prediction of 2.733 ± 0.001 as the critical aspect ratio compared with the numerically found value of 2.7 ± 0.05 . The second is the analytical prediction of a discontinuous transition between the leaf and the flower states without any metastability. This last point agrees with the numerical experiments for element thicknesses less than 12 nm.

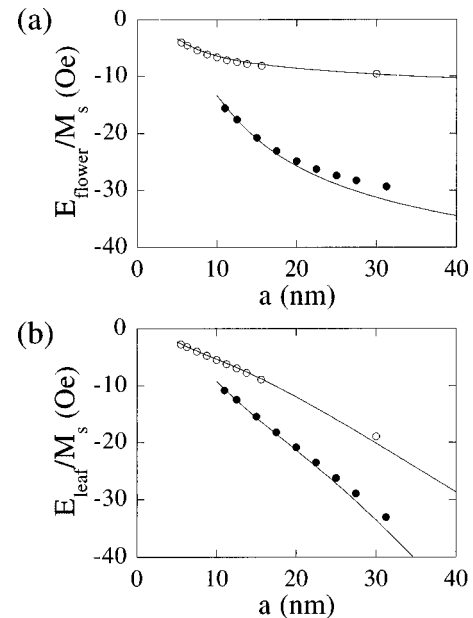


FIG. 8. A comparison between the equilibrium energy densities calculated by numerical simulation (open points indicate 5 nm thick, solid points indicate 10 nm thick) and the analytical model (lines) for different size elements. (a) is for the flower state and (b) is for the leaf state.

B. Limits of validity of the analytical model

There are two approximations which have been made in the analytical model. The first is that the equilibrium perturbation can be described by the functions $\Delta\phi(x,y)$ and $\Delta\theta(x,y,z)$ given by Eqs. (5) and (6). In reality, it is likely that the precisely required function would also involve higher-order polynomial terms. The second approximation has already been mentioned and is the fact that the demagnetizing field due to the *unperturbed* magnetization is taken as the internal field, whereas a precise calculation would use the demagnetizing field due to the *perturbed* magnetization. In failing to take this into account, one is ignoring the magnetostatic interaction between volume charges within the perturbed distribution.

The first approximation introduces the same proportional error for any size element (at fixed aspect ratio). This can be seen by the following. Suppose that there is a general perturbation $\Delta\phi(x/a,y/a,z/a)$ for which an element of side a_1 is in equilibrium, but which is not necessarily of the simple form of Eq. (5). At any point in the element, the exchange energy density is proportional to $|\text{grad}\Delta\phi(x/a,y/a,z/a)|^2$ and the magnetostatic energy density is proportional to $\Delta\phi(x/a,y/a,z/a)$ (in the limit of assumption 2 holding). Consider now another element of the same aspect ratio, but of side a_2 and consider the perturbation $(a_2/a_1)^2\Delta\phi(x/a,y/a,z/a)$ applied to it. The local magnetostatic energy density, being scale invariant, will be increased by a factor $(a_2/a_1)^2$. Because grad is a linear operator, the local exchange energy density will also be increased by a factor $(a_2/a_1)^2$. Thus, $(a_2/a_1)^2\Delta\phi(x/a,y/a,z/a)$ is the equilibrium distribution for the new element. In other words, as an element scales, the overall *shape* of its perturbation does not change, but only its magnitude. Thus if, say 10%, of the energy of an equilibrium distribution is due to a perturbation which is distributed according to x^5y^5 , then that proportion will not change as the element size is reduced.

The second approximation becomes increasingly accurate as the element size is reduced. Each volume charge is of magnitude proportional to $\Delta\phi$ and so the interaction energy between volume charges is proportional to $\Delta\phi^2$. Thus the relative error is proportional to $\Delta\phi$. Now we know from the previous paragraph that $\Delta\phi$ scales with a^2 and so the relative error scales with a^2 , vanishing for small elements. We estimate that an overall precision of 10% can be achieved in the analytical model as long as all of the perturbation strength parameters are less than approximation 20° (0.35 rad).

One of the curious differences between the analytical and numerical work is that the numerical simulations show an abrupt transition at the critical aspect ratio for element thicknesses less than 12 nm and a smooth transition for thicknesses greater than 12 nm. By contrast, the analytical model only contains absolute length scales as a final scaling factor, meaning that qualitative behavior can only depend upon the aspect ratio and not the absolute size. Inclusion of higher-order perturbations as described above would not change this. Correction of the second approximation could, however, introduce a change in qualitative behavior for different element sizes. More specifically, in order to predict a gradual transition, additional harmonic terms would be required in Eq. (16). Numerical results not shown here show that the

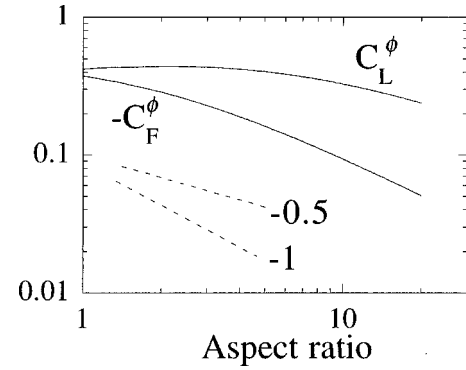


FIG. 9. The principal in-plane perturbation C factors plotted against width to thickness aspect ratio on a logarithmic scale. The dashed guide lines show gradients of -1 and -0.5 .

energy surface between the basis states does develop a term in $\sin^2 4\langle\phi\rangle$ for larger elements. Such a term (if, as it is, of the correct sign) would indeed break the abruptness of the transition from $\langle\phi\rangle=45^\circ$ to $\langle\phi\rangle=90^\circ$. It is not unreasonable to suppose that this higher harmonic appears because of the introduction of nonlinearity due to the second approximation breaking down, and as such is a finite-size effect. A corollary of this is that the real transition becomes rigorously abrupt, with the in-plane susceptibility diverging, in the limit of the element size tending to zero or alternatively the exchange length tending to infinity. Further work is required to see if this is strictly a first-order phase transition according to the renormalization group.

C. Physical interpretation

The major motivation for producing an analytical model was to gain insight into the physical processes driving the flower to leaf transition. One surprising result to come out of the model is the fact that the transition is *not* driven by out-of-plane perturbations. Equation (16) shows that there is a contribution to the total magnetic energy from the out-of-plane perturbation (via the term R) at least for small aspect ratios, but that it does not depend upon $\langle\phi\rangle$, i.e., which of the flower or leaf basis states is adopted.

It is the form of the C factor curves which gives the clue to the physical driving force. It is possible to show that in any equilibrium state the magnetostatic energy density is directly proportional to the total energy density. Thus, the magnetostatic energy density of the leaf state must exceed (in magnitude) that of the flower state for larger aspect ratios. Now the definition of the C factors given in Eq. (12) is such that they are directly proportional to the magnetostatic energy density of the perturbation. We have plotted C_F^ϕ and C_L^ϕ against aspect ratio in log-log form in Fig. 9. The guide gradient lines show that C_F^ϕ falls off approximately with $1/r$ at larger r whereas C_L^ϕ falls off with a lower power law, closer to $1/\sqrt{r}$. It is these different dependences which are at the heart of the flower to leaf transition. We can explain the dependences by considering the part of the sample which experiences the greatest perturbation and hence which contributes most to the overall magnetostatic energy density. For the flower, it is close to the corners, whereas for the leaf it is close to the middle of the edges. Now for the flower, the

magnetostatic energy of the perturbation depends upon *off*-diagonal demagnetizing tensor terms, and so the edge charges nearest to any given point inside the element do not contribute. Consequently, most of the edge charges which do contribute to the magnetostatic energy density at a point are far away from that point, i.e., in the far field and so the dependence on aspect ratio is simply $1/r$. Conversely, the magnetostatic energy of the leaf perturbation depends upon *diagonal* demagnetizing tensor terms, and so most of the magnetostatic energy density at a point is due to the nearest edge charges. These are mostly in the near field, and so the dependence on aspect ratio is of lower power than $1/r$. We can thus explain why there is a change over from flower to leaf ground state as the aspect ratio is increased.

D. Technological significance

One of the most striking findings of this work is the strength of the configurational anisotropy. Although due to a small perturbation from the uniform state, the configurational anisotropy field is very strong. Substituting the values for a $40\text{ nm} \times 40\text{ nm} \times 10\text{ nm}$ Permalloy element (which is the size future magnetoelectronic devices might use) into Eq. (21) gives an anisotropy field of 107 Oe, which is to be compared with the uniaxial anisotropy field of field cooled Permalloy of the order of 4 Oe.²⁰ Elements of the same thickness but of larger lateral size, which will most probably find technological application first, will have an even stronger anisotropy field, although the analytical model is not quantitatively valid for these large perturbations. There are two consequences of this. Firstly, the remanent magnetization will point along the diagonals, reducing say the giant magnetoresistance response by one half. Secondly, and perhaps most significantly, the element switching field will be much greater than it otherwise would have been. Higher write currents will therefore be needed, leading to increased power dissipation.

Conversely, our work shows that square elements which are 2.7 times wider than they are thick should be isotropic (in-plane). They should thus have an extremely high susceptibility which can be tuned by simply varying the aspect ratio and which could find important applications in magnetic sensors.

CONCLUSION

We have studied theoretically the energy surface in the vicinity of the two equilibrium near single domain states of nanoscale square-planar magnetic elements (magnetic nanostructures). We find from numerical simulations that metastability is absent and at any finite temperature the system must adopt its ground state.

We have then modeled the flower and leaf states analytically as small perturbations from the uniformly magnetized state. We find that the energy surface between the states can be described by a fourfold symmetric configurational anisotropy field which changes sign at a critical width to thickness aspect ratio. We have derived an equation predicting the strength of the configurational anisotropy as a function of element size and thickness, obtaining excellent agreement with the numerical simulations for the value of the critical aspect ratio. We find that the configurational anisotropy field can be several hundred Oe's in strength, which will dominate the spin-reversal process and which may have other technological implications. The analytical model allows important physical quantities of the nanostructures such as energy and anisotropy to be rapidly calculated without performing long numerical simulations. More importantly, however, it gives good insight into the physical origin of the configurational anisotropy. The leaf energy density falls off less rapidly with increasing aspect ratio than the flower energy density because the former involves mainly near field demagnetizing terms whereas the latter involves mainly far field terms. Out-of-plane perturbations are found to be unimportant in selecting between the two states. The analytical model itself predicts a discontinuous transition to occur at the critical aspect ratio. The approximations used by the model are such that this will become rigorously valid in the limit of the infinite exchange length or zero element size.

ACKNOWLEDGMENTS

This work was supported by St. John's College, Cambridge, The Royal Society, and EU ESPRIT Nanowires. We are grateful to Dr. A. Thiaville for helpful discussions.

*Electronic address: rpc12@cus.cam.ac.uk

¹B. Heinrich and J. A. C. Bland, *Ultrathin Magnetic Structures* (Springer-Verlag, Berlin, 1994).

²M. Hehn, K. Ounadjela, J. P. Bucher, F. Rousseaux, D. Decanini, B. Bartenlian, and C. Chappert, *Science* **272**, 1782 (1996); E. Gu, E. Ahmad, S. J. Gray, C. Daboo, J. A. C. Bland, L. M. Brown, M. Rühlig, A. J. McGibbon, and J. N. Chapman, *Phys. Rev. Lett.* **78**, 1158 (1997); K. J. Kirk, J. N. Chapman, and C. D. W. Wilkinson, *Appl. Phys. Lett.* **71**, 539 (1997); R. P. Cowburn, A. O. Adeyeye, and J. A. C. Bland, *ibid.* **70**, 2309 (1997); C. Beeli, B. Doudin, and P. Stadelmann, *Phys. Rev. Lett.* **75**, 4630 (1995); T. Ono, H. Miyajima, K. Shigeto, and T. Shinjo, *Appl. Phys. Lett.* **72**, 1116 (1998); P. Holody, L. B. Steren, R. Morel, A. Fert, R. Loloee, and P. A. Schroeder, *Phys. Rev. B* **50**, 12 999 (1994).

³L. Landau and E. Lifschitz, *Phys. Z. Sowjetunion* **8**, 153 (1935); W. F. Brown, *Micromagnetics* (Wiley, New York, 1963).

⁴A. Aharoni, *Introduction to the Theory of Ferromagnetism* (Ox-

ford University Press, Oxford, 1996).

⁵W. Williams and D. J. Dunlop, *Nature* (London) **337**, 634 (1989); M. E. Schabes and H. N. Bertram, *J. Appl. Phys.* **64**, 1347 (1988); D. R. Fredkin and T. R. Koehler, *ibid.* **67**, 5544 (1990); N. A. Usov and S. E. Peschany, *J. Magn. Magn. Mater.* **110**, L1 (1992); H. F. Schmidts and H. Kronmüller, *ibid.* **130**, 329 (1994).

⁶S. W. Yuan, H. N. Bertram, J. F. Smyth, and S. Schultz, *IEEE Trans. Magn.* **28**, 3171 (1992); J. G. Zhu, Y. F. Zheng, and X. D. Lin, *J. Appl. Phys.* **81**, 4336 (1997); H. N. Bertram and J.-G. Zhu, in *Solid State Physics: Advances in Research and Applications*, edited by H. Ehrenreich and D. Turnbull (Academic, New York, 1992).

⁷Y. F. Zheng and J. G. Zhu, *IEEE Trans. Magn.* **32**, 4237 (1996); K. M. Tako, M. A. Wongsam, and R. W. Chantrell, *J. Magn. Magn. Mater.* **155**, 40 (1996).

⁸W. F. Brown, Jr., *J. Appl. Phys.* **39**, 993 (1968).

⁹A. Aharoni, *Phys. Rev. B* **45**, 1030 (1992).

- ¹⁰R. P. Cowburn and M. E. Welland, Appl. Phys. Lett. **72**, 2041 (1998).
- ¹¹S. Y. Chou, Proc. IEEE **85**, 652 (1997).
- ¹²M. Johnson, J. Magn. Magn. Mater. **156**, 321 (1996); G. Prinz and K. Hathaway, Phys. Today **48** (4), 24 (1995).
- ¹³W. F. Brown, Jr., Rev. Mod. Phys. **17**, 15 (1945); U. Hartmann, Phys. Rev. B **36**, 2331 (1987).
- ¹⁴M. E. Schabes and A. Aharoni, IEEE Trans. Magn. **23**, 3882 (1987); A. Aharoni, *ibid.* **27**, 3539 (1991).
- ¹⁵W. F. Brown, Jr., J. Appl. Phys. **39**, 993 (1968); W. F. Brown, Jr., Ann. (N.Y.) Acad. Sci. **147**, 461 (1969); A. Aharoni, J. Appl. Phys. **63**, 5879 (1988).
- ¹⁶W. F. Brown, Jr., Phys. Rev. **105**, 1479 (1957).
- ¹⁷R. L. Joseph and E. Schlömann, J. Appl. Phys. **36**, 1579 (1965).
- ¹⁸S. T. Chui and V. N. Ryzhov, Phys. Rev. Lett. **78**, 2224 (1997).
- ¹⁹W. Rave, K. Ramstöck, and A. Hubert, J. Magn. Magn. Mater. **183**, 329 (1998).
- ²⁰S. Chikazumi, *Physics of Magnetism* (Krieger, Malabar, Florida, 1978), p. 363.